Processing and Application of Ceramics 12 [3] (2018) 287–294
https://doi.org/10.2298/PAC1803287S

Studies on the hydrothermal synthesis of $Cd_xZn_{1-x}S$ compounds

Paula Svera[1,2], Daniel Niznansky[3], Mariana Nela Stefanut[1], Daniel Ursu[1], Paula Sfirloaga[1], Anamaria Dabici[1], Bogdan-Ovidiu Taranu[1], Ana-Maria Putz[4,*], Viorel-Aurel Serban[2]

[1]*National Institute for Research and Development in Electrochemistry and Condensed Matter, Dr. A.P. Podeanu no. 144, 300254 Timisoara, Romania*
[2]*Politehnica University of Timisoara, Department of Materials Manufacturing and Engineering, B-dul Mihai Viteazul no. 1, 300222 Timisoara, Romania*
[3]*Department of Inorganic Chemistry, Faculty of Science, Charles University in Prague, Hlavova 2030/8, 128 43 Prague 2, Czech Republic*
[4]*Institute of Chemistry Timisoara of Romanian Academy, Bvd. Mihai Viteazul no. 24, 300223 Timisoara, Romania*

Received 24 February 2018; Received in revised form 3 June 2018; Received in revised form 7 July 2018; Accepted 23 August 2018

Abstract

In this study series of $Cd_xZn_{1-x}S$ solid solutions with different amounts of Cd and Zn were synthesized by the hydrothermal treatment of aqueous solutions containing $CdCl_2$, $Na_2S \cdot 9\,H_2O$ and $ZnSO_4 \cdot 7\,H_2O$. The aim was to examine the influence of Zn concentration and processing conditions (hydrothermal temperature and duration) on the structure of the obtained powders and their photocatalytic activity (in water splitting process). The obtained photocatalysts (with and without Pd co-catalyst) were analysed by X-ray diffraction (XRD), atomic absorption spectroscopy (AAS), ultraviolet-visible spectroscopy (UV-VIS), scanning electron microscopy (SEM), transmission electron microscopy (TEM), Brunauer-Emmett-Teller (BET) method and gas chromatography (GC). The XRD results confirmed the crystallinity of the compounds and transition from hexagonal to cubic phase with increasing Zn content. Complete transformation from hexagonal to cubic phase did not take place, and both phases were present in almost all samples. BET analysis showed the importance of the pore distribution and pore size, especially in the case of photocatalysts with different duration treatment. GC measurements of the photocatalysts without and with Pd co-catalyst confirmed the production of hydrogen for all tested compounds. The best photocatalytic performance was achieved by the sample Zn_{50}230/72-Pd prepared at 230 °C, for 72 hours, with 50% Zn and in the presence of Pd co-catalyst. The synthesis implied neither stabilizer nor organic compound.

Keywords: *water splitting, $Cd_xZn_{1-x}S$, semiconductors, photocatalytic activity, hydrothermal*

I. Introduction

Hydrogen is currently a promising candidate for energy consumption regarding the zero emission pollution in combination with unlimited solar energy [1,2]. Still there are challenges regarding undesirable electron transfer loss, over-potential and instability of the photocatalytic materials [3]. Recurring disadvantages lead to different approaches with the aim to accelerate the charge separation and migration in the photocatalytic process, resulting in multiple studies on different types of materials [1,3,4–8].

Taking into account the efficiency, cadmium combined with zinc is widely used in water splitting experiments [9–11] in form of core shell [6], multiple systems [4,5] or doped with co-catalyst [2,7,8,12]. Other important features of this type of material represent the possibility to control the shape and size of the final photocatalysts by preparation methods like sol-gel, solvothermal, hydrothermal, chemical precipitation, micro-emulsion, inverse micelles and other methods [13,14]. Mixture between cadmium sulphide and zinc sulphide reflects

*Corresponding authors: tel: +40 723 088 129,
fax: +40 256 491 824, e-mail: *lacramaanamaria@yahoo.com*

similarities in crystalline structure [5,6]. Thus, combined with proper differences like band gap, results in wider band gap for Zn compared to Cd, in which Zn plays the role of the passivation surface material [6]. Also, it was observed from other studies that d^0 and d^{10} semiconductors are suitable for water splitting. It is yet another good characteristic of the selected materials in this study [2,8]. ZnS is a typical semiconductor with fully filled 3*d* shell (d^{10} configuration); it is colourless, since no *d*-*d* electronic transitions are possible; CdS has also fully filled 4*d* shell (d^{10} electronic configuration), but in this case the colour cannot be explained on the basis of crystal field theory and its resulting yellow colour is due to its semiconductor behaviour [8,15]. It was reported that electron transition energy for cadmium sulphide is 2.4 eV, which corresponds to the wavelength of 517 nm, absorbing all photons with energies of 2.4 eV or higher. This includes all the blue-violet region of the spectrum, as well as green, resulting in yellow coloured material [8,10]. In order to shift the absorption edge of ZnS (3.6 eV) into the visible range, studies regarding $Cd_xZn_{1-x}S$ compounds formed by substitution of Zn^{2+} with Cd^{2+}, or by incorporation of ZnS into the structure of CdS began to have more importance recently [10,11,14]. Besides the compound concentration variation, other properties such as the crystal structure, size, shape, specific area and surface defect states play important role [11,16].

In the current study, series of $Cd_xZn_{1-x}S$ solid solutions with different amounts of Cd and Zn were hydrothermally prepared at different temperatures and duration and tested under visible light in Na_2S/Na_2SO_3 solution with and without Pd co-catalyst. $ZnSO_4 \cdot 7\,H_2O$ was used as zinc precursor instead of nitrates and no stabilizer neither organic compound was added. To the best of our knowledge, Zn precursor used in this synthesis was not reported in previous papers concerning photocatalytic water splitting of $Cd_xZn_{1-x}S$ compounds.

II. Experimental procedure

2.1. Materials

All used materials ($CdCl_2 \cdot 2.5\,H_2O$, $Na_2S \cdot 9\,H_2O$, $ZnSO_4 \cdot 7\,H_2O$, Na_2SO_3, $PdCl_2$) were of analytical grade and purchased from Sigma-Aldrich. Deionized water was used during all the experiments. Standards like nitric acid 67% (Merck, free of heavy metals), Zink-Standardlösung (1.19806.0100, CertiPUR®, Merck) and Cadmium-Standardlösung (1.19777.0100, CertiPUR®, Merck) were used for atomic absorption spectroscopy analyses.

2.2. $Cd_xZn_{1-x}S$ synthesis

Different concentrations of $CdCl_2 \cdot 2.5\,H_2O$ were mixed with $Na_2S \cdot 9\,H_2O$ and 20 ml of water. The mixture was then left under sonication for 5 minutes. After the sonication $ZnSO_4 \cdot 7\,H_2O$ was added to the mixture. After the second sonication, the mixture was transferred into a teflon-lined stainless steel autoclave and treated hydrothermally at different temperatures and times, as shown in the Table 1. After the hydrothermal treatment, autoclaves were cooled down to room temperature and the obtained mixture was washed and filtered several times with water and dried at 80 °C for 8 hours. Pd source (1 M $PdCl_2$ solution) was added at room temperature after the synthesis.

2.3. Characterization

The phase purity was studied using powder X-ray diffraction (XRD) on Panalytical X'Pert PRO MPD diffractometer. Concentration ratio of Cd/Zn in compounds was determined by atomic absorption spectroscopy (AAS) on novAA 400G Analytik Jena aparatus. Optical characterization was performed by Perkin Elmer, Lambda 950 UV-VIS Spectrophotometer. The morphology of the materials was investigated by scanning electron microscopy (SEM) using FEI Inspect S and transmission electron microscopy (TEM) using FEI Titan G2 80-200 transmission electron microscope (operating at 200 keV). The specific surface area and pore size distribution data were determined by low temperature nitrogen adsorption using QUANTACHROME Nova 1200 apparatus and Brunauere-Emmette-Teller (BET) and Barrette Joynere-Halenda (BJH) methods, respectively. All samples were initially degassed in vacuum at room temperature for 12 h. H_2 detection was performed by gas-chromatography (GC) using Chromatron Gas-Chromatograph GCHF 18.3.

2.4. Photocatalytic process and reactor

All photocatalysts were tested in a Pyrex glass reactor connected to the gas-chromatograph by a loop and the measurements were taken on every hour. The $Cd_xZn_{1-x}S$ photocatalyst (0.05 g) was dispersed in a 100 ml aqueous solution containing 0.4 M $Na_2S \cdot 9\,H_2O$ and 0.2 M Na_2SO_3, which served as sacrificial agents. By combination of SO_3^{2-} and S^{2-}, utilized as sacrificial agent, specific reactions occurred [1,11]:

$$Cd_xZn_{1-x}S + h\nu \rightarrow h^+ + e^-$$

$$e^- + 2\,H_2O \rightarrow H_2 + 2\,OH^-$$

$$SO_3^{2-} + 2\,OH^- + 2h^+ \rightarrow SO_4^{2-} + 2\,H^+$$

$$2\,S^{2-} + 2h^+ \rightarrow S_2^{2-}$$

$$S_2^{2-} + SO_3^{2-} \rightarrow S_2O_3^{2-} + S^{2-}$$

$$SO_3^{2-} + S^{2-} + 2h^+ \rightarrow S_2O_3^{2-}$$

The first measurement (zero measurement) was taken after several system purging with vacuum and argon. The second measurement was taken after one hour of reactor illumination with 300 W xenon lamp. Measurements lasted 6 hours and during entire experiment the photocatalysts inside the reactor were stirred and kept at constant temperature. In case of Zn_{50}230/72-Pd, Zn_{50}230/12-Pd and Zn_{50}150/12-Pd

Table 1. Synthesis parameters of obtained photocatalysts

Sample	$CdCl_2 \cdot 2.5\,H_2O$ [mmol]	$ZnSO_4 \cdot 7\,H_2O$ [mmol]	$Na_2S \cdot 9\,H_2O$ [mmol]	T_{HT} [°C]	τ_{HT} [h]	$PdCl_2$ co-catalyst [mmol]
$Zn_2$150/12	1.96	0.04	2.29	150	12	-
$Zn_5$150/12	1.9	0.1	2.30	150	12	-
Zn_{10}150/12	1.8	0.2	2.29	150	12	-
Zn_{20}150/12	1.6	0.4	2.29	150	12	-
Zn_{40}150/12	1.2	0.8	2.29	150	12	-
Zn_{50}150/12	1	1	2.30	150	12	-
Zn_{60}150/12	0.8	1.2	2.30	150	12	-
Zn_{50}100/12	1	1	2.30	100	12	-
Zn_{50}200/12	1	1	2.30	200	12	-
Zn_{50}230/12	1	1	2.30	230	12	-
Zn_{50}230/6	1	1	2.30	230	6	-
Zn_{50}230/24	1	1	2.30	230	24	-
Zn_{50}230/48	1	1	2.30	230	48	-
Zn_{50}230/72	1	1	2.30	230	72	-
Zn_{50}150/12-Pd	1	1	2.30	150	12	1
Zn_{50}230/12-Pd	1	1	2.30	230	12	1
Zn_{50}230/72-Pd	1	1	2.30	230	72	1

photocatalysts, 1 ml of 1 M $PdCl_2$ solution was added to photocatalyst/$Na_2S \cdot 9\,H_2O$/Na_2SO_3 mixture at room temperature before the system was cleaned with vacuum/argon and before the first GC measurement.

III. Results and discussion

3.1. XRD analyses

XRD patterns show a size-broadening effect which demonstrates the finite size of the synthesized $Cd_xZn_{1-x}S$ nanocrystals. During the analysis, three crystal phases were identified corresponding to the standard XRD patterns of the cubic ZnS (JCPDS No. 00-005-0566), cubic CdS (JCPDS No. 00-002-0454) and hexagonal CdS (JCPDS No. 00-001-0780) represented at the bottom of Figs. 1, 2 and 3 [14]. The XRD peaks of CdS/$Cd_xZn_{1-x}S$ clusters gradually shift to larger angles and the phase transformation from hexagonal to cubic

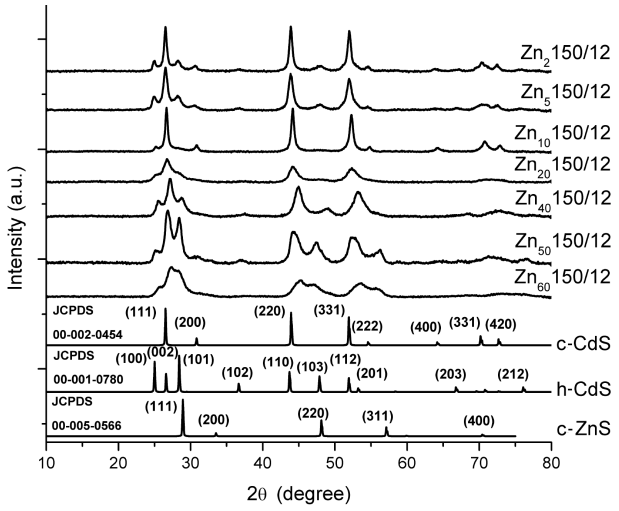

Figure 1. XRD measurements of photocatalysts with different Zn concentration

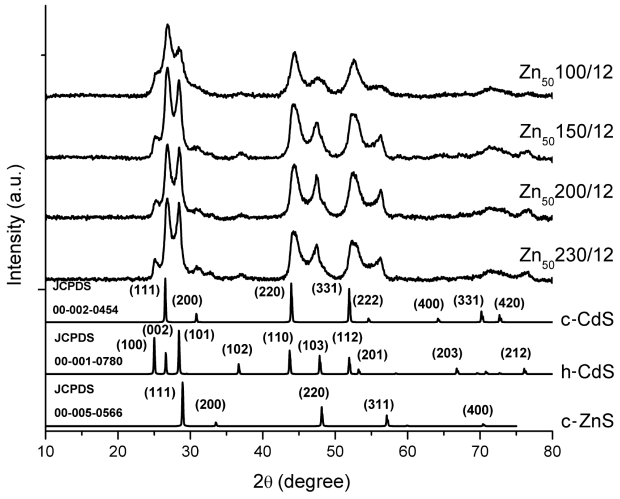

Figure 2. XRD measurements of photocatalysts at different thermal treatment temperature

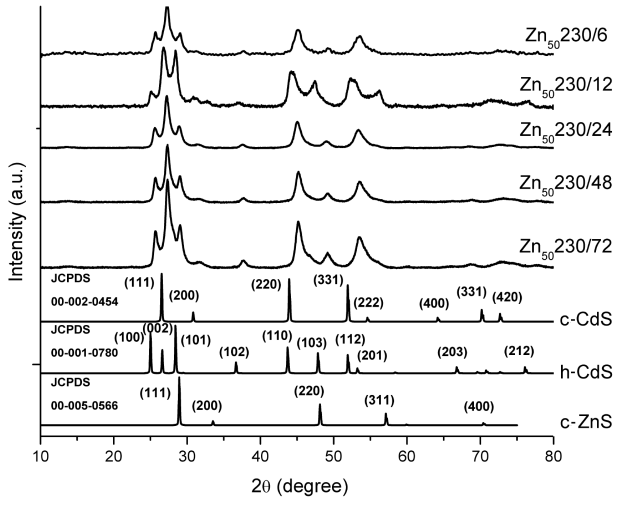

Figure 3. XRD measurements of photocatalysts at different duration of thermal treatment

can be observed with increasing Zn content (Fig. 1). Complete transformation from hexagonal to cubic phase did not take place, and both phases were present in almost all samples. The predominant cubic phase ends at sample with 60% Zn (Zn_{60}150/12). The continuous peak shift of CdS/$Cd_xZn_{1-x}S$ clusters also indicates that there is no phase separation or separated nucleation of ZnS or CdS in $Cd_xZn_{1-x}S$ clusters [11].

The increase of temperature in hydrothermal synthesis influences the structure of the materials by increasing the percentage of cubic phase and decreasing the amount of hexagonal phase (Fig. 2). Zn_{50}200/12 shows the most dominant cubic sphalerite phase along with hexagonal wurtzite phase implying that both phases coexist in all the samples treated at different thermal conditions.

When comparing samples with different duration of hydrothermal treatment (Fig. 3), small variations were observed in the case of 28.30° XRD peak, which corresponds to specific (101) plane.

3.2. Atomic absorption spectrometry

Preparation for the analysis implied different quantities of the photocatalyst (0.02–0.04 g weighted with 0.00001 g precision), which were digested with 5.5 ml HNO_3 using a MWS-2 Berghof oven (1000 W). Calibration curves were made for Zn and Cd (presented on request). The obtained results (Table 2) show different values from the initially introduced concentrations of the precursors before the hydrothermal treatment (Table 1), which could be attributed to the nucleation effect during the exposure to higher temperature.

Table 2. Concentrations of Cd and Zn in photocatalysts and corresponding Cd/Zn ratio

Sample	Cd [mmol]	Zn [mmol]	Cd/Zn ratio
Zn_{50}150/12	0.206	0.181	1.14
Zn_{50}230/12	0.126	0.150	0.84

3.3. UV-VIS spectroscopy

The absorbance spectra of $Cd_xZn_{1-x}S$ materials with different compositions and prepared at different conditions (hydrothermal temperature and duration), were presented in Figs. 4, 5 and 6. All absorption edges of the analysed materials are placed in the visible region with the tendency to shift closer to the infrared region due to the increase of Cd content (Fig. 4), as confirmed by related study [9]. The CdS and ZnS absorption wavelengths are clearly seen at 510 nm and 340 nm, respectively. In addition, higher absorption and movement of the characteristic band closer to 510 nm are obvious for the compound containing more Cd [17]. In the case of the materials synthesized under different thermal treatments, the shift in the UV direction was observed with the increase of temperature (Fig. 5) and decrease of duration of hydrothermal treatment (Fig. 6).

From UV-VIS absorbance data, using Tauc plot [18],

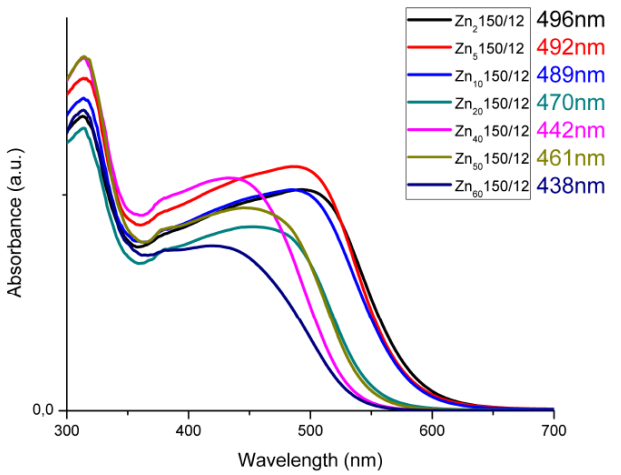

Figure 4. Variations of optical absorption wavelengths of $Cd_xZn_{1-x}S$ with increasing Zn concentration

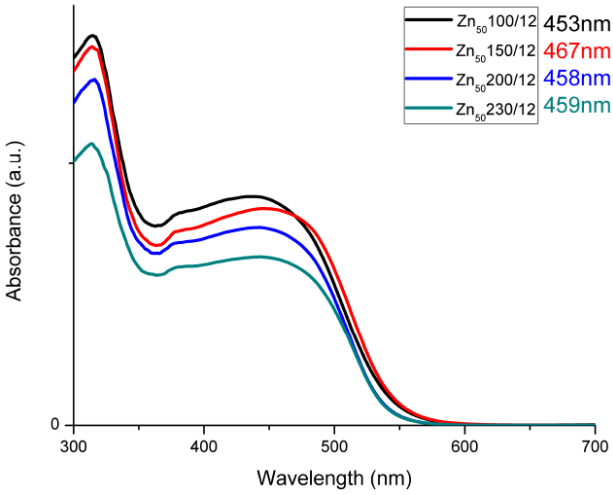

Figure 5. Variations of optical absorption wavelengths of $Cd_xZn_{1-x}S$ with increasing thermal treatment temperature

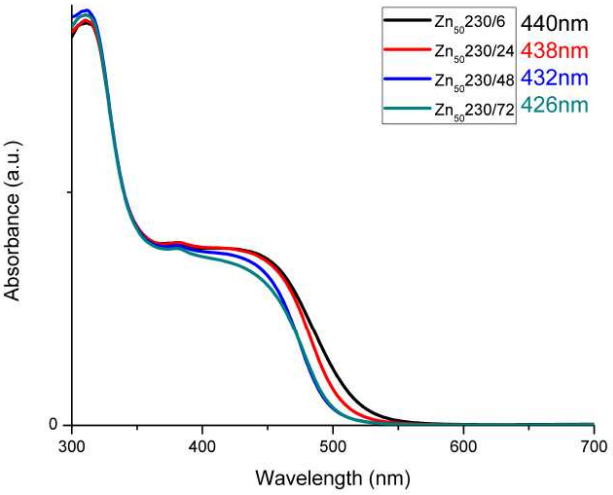

Figure 6. Variations of optical absorption wavelengths of $Cd_xZn_{1-x}S$ with increasing hydrothermal duration

the band gap values were obtained. The band gap values could be used to predict the hydrogen production capacity of the materials and improve the prepared photocatalysts. The determined energy band gaps of the photocatalysts (Figs. 7, 8 and 9) varied from 2.20 to 2.53 eV. The increase is attributed to the Zn content which is confirmed by previous analyses and only the sample $Zn_{50}150/12$ presented slight deviation from the encountered tendency of the photocatalysts.

3.4. N_2 adsorption desorption isotherms

Low-temperature N_2 adsorption of the analysed samples was performed at 77 K and the specific surface area and pore size distribution were determined using BET and BJH methods (Table 3). The highest specific surface area among the compounds in the first catergory with different Zn concentrations ($Zn_2150/12$, $Zn_5150/12$, $Zn_{10}150/12$, $Zn_{20}150/12$, $Zn_{40}150/12$, $Zn_{50}150/12$ and $Zn_{60}150/12$) was registered in the case of $Zn_{50}150/12$ (76.0 m^2/g). The photocatalyst $Zn_{20}150/12$ has the lowest specific surface area (27.5 m^2/g) and total pore volume. The pore size distribution values (d_{BJHads} and d_{BJHdes}) indicate disordered porosity for all compounds, except for $Zn_{50}150/12$ with the lowest value difference between d_{BJHads} and d_{BJHdes}, and simultaneously the lowest porosity disorder. According to the pore width values (d_{DFT}), only mesopores are present in the samples. Fractal dimension values (ds_{FHH}) demonstrate almost similar rugosity among all the samples.

The analyses of the samples from the second category, which includes different hydrothermal temperature ($Zn_{50}100/12$, $Zn_{50}150/12$, $Zn_{50}200/12$, $Zn_{50}230/12$) highligth that $Zn_{50}230/12$ has the highest specific surface area of 74.7 m^2/g and the lowest one the sample $Zn_{50}100/12$ (23.6 m^2/g). Pore size distribution and rugosity were not influenced by temperature of the hydrothermal treatment, and stayed almost unchanged in comparison to the previous category. It should be observed that the temperature significantly influences the total pore volume and specific surface area. The sample Zn50230/12 is characterized by the ordered porosity which is not the case for the rest of the samples.

When comparing samples with different duration of the hydrothermal treatment (the third category: $Zn_{50}230/6$, $Zn_{50}230/24$, $Zn_{50}230/48$, $Zn_{50}230/72$), it can be observed that, with the increased duration, the specific surface area and total pore volume decrease while the pore size calculated by DFT method and rugosity slightly increase. $Zn_{50}230/48$ and $Zn_{50}230/72$ exhibit ordered porosity with $Zn_{50}230/72$ having more ordered pores in comparison to $Zn_{50}230/48$.

The above observations correspond to the literature, explaining the close connection between the increase of surface area and increment of the active sites number along with the surface defects [11]. This phenomenon is defined by the presence of electron-hole pairs that are separated and transferred on the catalyst surface, taking part in water splitting reaction. It was concluded that the

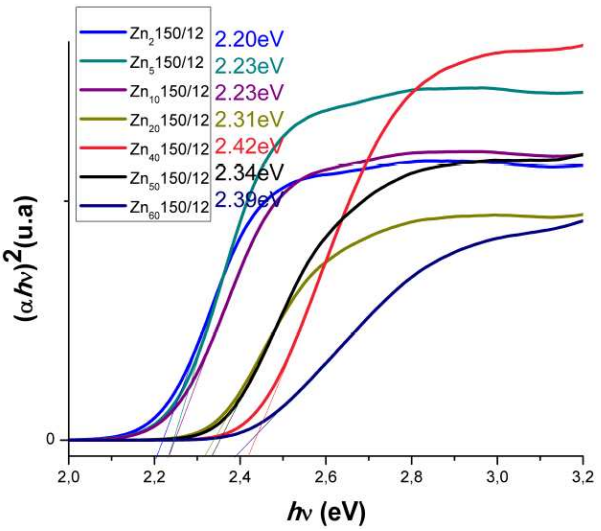

Figure 7. Calculated band gap of $Cd_xZn_{1-x}S$ with different Zn concentrations

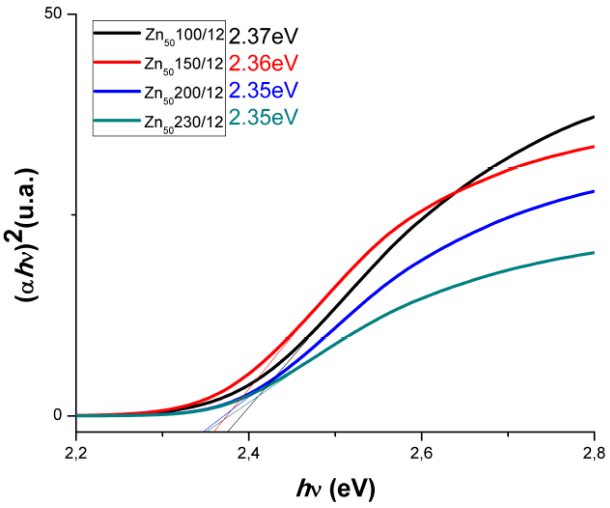

Figure 8. Calculated band gap of $Cd_xZn_{1-x}S$ prepared at different temperatures

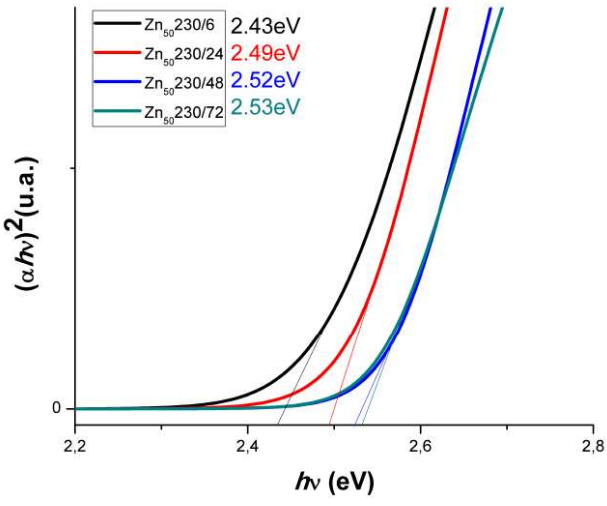

Figure 9. Calculated band gap of $Cd_xZn_{1-x}S$ prepared under different hydrothermal duration

Table 3. Surface and textural characteristics obtained from adsorption-desorption isotherms (DFT and BJH methods)

Sample	S_{BET} [m^2/g]	d_{DFT} [nm]	d_{BJHads} [nm]	d_{BJHdes} [nm]	VTP [cm^3/g]	ds FHH
$Zn_2$150/12	36.8	28.3	31.8	25.3	0.20	2.37
$Zn_5$150/12	51.6	14.4	23.3	12.6	0.23	2.37
Zn_{10}150/12	27.5	18.5	32.0	17.9	0.16	2.38
Zn_{20}150/12	45.3	5.8	8.9	3.7	0.14	2.49
Zn_{40}150/12	56.6	13.9	23.0	12.5	0.25	2.38
Zn_{50}150/12	76.0	8.7	6.1	3.7	0.18	2.52
Zn_{60}150/12	66.7	9.4	15.1	12.4	0.26	2.41
Zn_{50}100/12	23.6	17.2	3.6	24.3	0.08	2.51
Zn_{50}200/12	31.0	18.5	23.5	17.9	0.15	2.43
Zn_{50}230/12	74.7	9.4	8.7	8.9	0.25	2.45
Zn_{50}230/6	40.7	18.5	3.4	24.9	0.22	2.47
Zn_{50}230/24	29.1	18.5	3.4	24.8	0.13	2.54
Zn_{50}230/48	29.0	20.0	3.0	3.7	0.10	2.53
Zn_{50}230/72	25.0	20.0	3.0	3.2	0.07	2.55

higher specific area, the more active sites are present, resulting in successful water splitting reaction [11,12]. Because the presence of the defects cannot be demonstrated by BET, they could be explained by the presence of both cubic and hexagonal phases in XRD. The importance of the surface defects is reflected on the ability to capture photogenerated electrons or holes, and as a consequence, an intensified migration of electron/ hole to the surface of the catalyst, leading to a successful photocatalytic reaction. However, the porosity disorder was not evidenced in other studies, revealing an important factor that could affect the water splitting process and simultaneously the H_2 production. High specific surface areas were accompanied by the ordered porosity in two categories (the samples with different Zn concentrations and different temperatures of the hydrothermal treatment). A deviation is observed in the case of the third category (compared by the hydrothermal duration) resulting in lower surface area, but high ordered porosity with the increase of thermal duration.

3.5. SEM and TEM analyses

In Fig. 10 the morphological analyses of the investigated samples are presented. The photocatalyst particles are distributed randomly and form cluster agglomerates. SEM images (Fig. 10) of the prepared photocatalysts

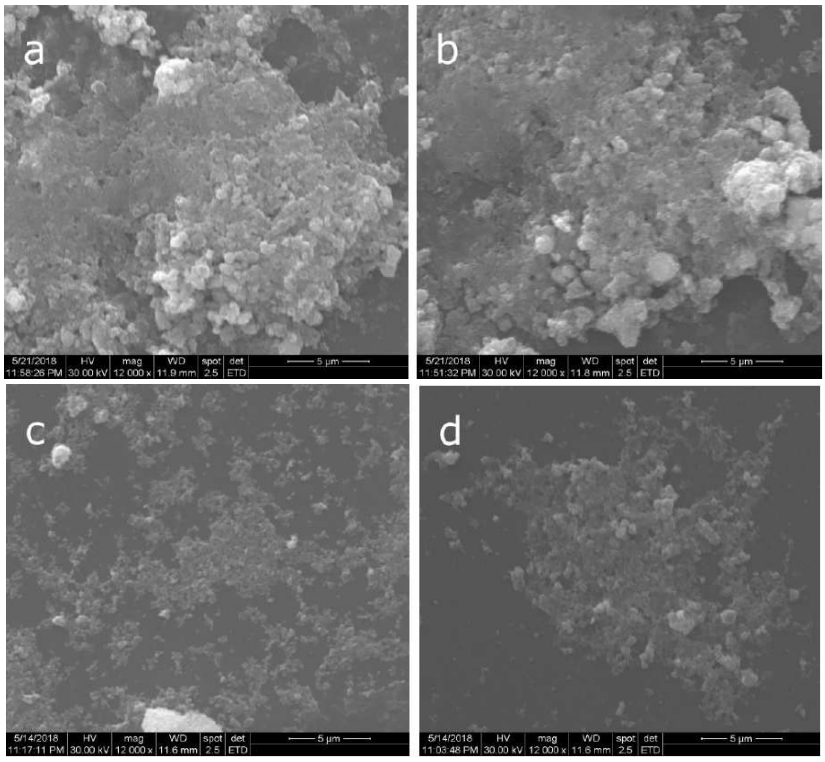

Figure 10. SEM morphology of photocatalysts with different Zn contents: Zn_{50}150/12 (a) and Zn_{10}150/12 (b), and different temperatures of the hydrothermal treatment: Zn_{50}230/12 (c) and Zn_{50}100/12 (d)

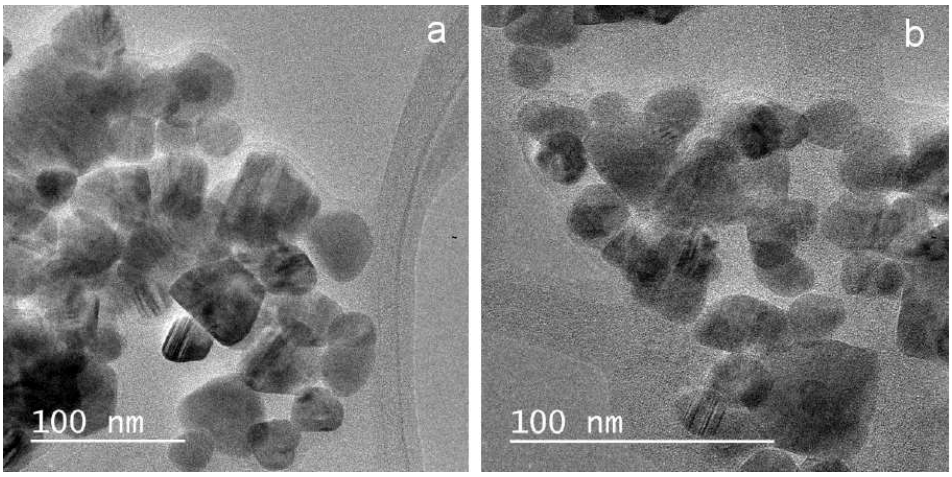

Figure 11. TEM morphology for Zn_{50}230/72 (a) and Zn_{50}230/6 (b) from photocatalysts with different treatment duration

suggest decrease in the size of the agglomerates when exposed to higher temperatures compared to the samples with different Zn concentrations. The morphology of all analysed materials is roughly spherical.

TEM images (Fig. 11) confirm the presence of quasi-spherically shaped grains with different sizes. TEM images show nanocrystallites with the average size of ~20 and ~30 nm in case of the samples Zn_{50}230/6 and Zn_{50}230/72, respectively. Aggregation of these crystallites results in apparently bigger particles with larger diameters which could be seen in SEM images (Fig. 10) [19]. Other feature is the strip like structure that appears on the surface of the nanoparticles due to the hydrothermal treatment resulting in stacking faults, characteristic for close-packed structures, or nano-twins [20]. It was also observed that the particles are merging which could confirm the nucleation that occurs in AAS results.

3.6. Gas chromatography measurements

All three categories of the photocatalysts were tested by GC highlighting the parameters that influence the photocatalytic performance. According to the obtained results, there were no other peaks except the specific peak for H_2. All measurements lasted for 6 hours, starting with the measurement zero in the absence of the light and with previous vacuum and argon system cleaning. H_2 value (in micromoles) was obtained by multiplication of the peak area and calculated correction factor. Considering the volatility of H_2, the gas chromatography measurements were performed directly by connecting the reactor and apparatus. In consequence there is an empty space which was taken into account, in order to obtain correct H_2 value. As mentioned, final H_2 value ($H_{2\,final}$) was calculated by multiplication of loop volume (V_l) and empty space between reactor and loop total volume (V_t) accordingly to the formula (1):

$$H_{2\,final} = H_2 \cdot V_t / V_l \quad (1)$$

From the obtained GC measurements (Table 4), Zn_{50}150/12 exhibited the highest H_2 production rate among photocatalysts with different Zn composition.

Table 4. H_2 values obtained from GC measurements

Sample	H_2 [mmol g^{-1} h^{-1}]
$Zn_2$150/12	0.028
Zn_{10}150/12	0.013
Zn_{20}150/12	0.024
Zn_{50}150/12	0.128
Zn_{60}150/12	0.125
Zn_{50}100/12	0.032
Zn_{50}200/12	0.412
Zn_{50}230/12	0.543
Zn_{50}230/6	0.275
Zn_{50}230/24	0.320
Zn_{50}230/48	0.634
Zn_{50}230/72	0.702
Zn_{50}150/12-Pd	0.569
Zn_{50}230/12-Pd	2.726
Zn_{50}230/72-Pd	1.987

The Zn_{50}150/12 was improved by increasing the synthesis temperature, therefore Zn_{50}230/12 exhibited higher results with H_2 production rate of 0.54 mmol g^{-1} h^{-1}. Co-catalysts have positive effect on the water splitting process, which have been discussed in many studies and Pt being the most used one. The present study showed good results by introducing Pd in the compound reflecting positive outcome and also being the cheapest noble metal [12]. Consequently, Zn_{50}230/12-Pd doped with Pd obtained H_2 production rate of 0.56 mmol g^{-1} h^{-1}, which was slightly above Zn_{50}230/12 sample. In order to improve the existing material, Zn_{50}230/12 was left longer under the hydrothermal treatment, resulting Zn_{50}230/72 as the most favourable photocatalyst in this category with 0.70 mmol g^{-1} h^{-1} H_2 production rate. Zn_{50}230/72-Pd was expected to surpass the Zn_{50}230/12-Pd. However, better results were obtained by Zn_{50}230/12-Pd in the presence of Pd with 2.72 mmol g^{-1} h^{-1}. This effect could be linked with the surface and textural characteristics that showed lower total pore volume in the case of Zn_{50}230/72 when compared to Zn_{50}230/12. The most important factor is how-

ever the difference between specific surface area, which is much higher in the case of Zn_{50}230/12.

The influence of the specific surface area over the H_2 production rate was observed also in the case of $Cd_{0.2}Zn_{0.8}S$ microspheres reported by Wang *et al.* [11]. Even higher H_2 production rate was reached when 1 wt.% of Pt was loaded on $Cd_{0.2}Zn_{0.8}S$, which in our case was replaced with Pd [11]. Resulting values were merely influenced by the specific surface area which is responsible for surface defects and therefore higher number of reaction sites [11,21].

IV. Conclusions

In this study series of $Cd_xZn_{1-x}S$ solid solutions with different amounts of Cd and Zn were synthesized by the hydrothermal treatment of aqueous solutions containing $CdCl_2$, $Na_2S \cdot 9\,H_2O$ and $ZnSO_4 \cdot 7\,H_2O$. Strong influence of synthesis conditions (Zn concentration, hydrothermal temperature and duration) on specific surface area and pore structure was observed, while there are only slight changes in particle size and morphology. All hydrothermally synthesised materials performed photocatalytic activity confirmed by gas chromatography measurements and the presence of only one gas, H_2. Among the obtained materials, Zn_{50}230/72-Pd showed the best value with 2.72 mmol g^{-1} h^{-1}. The best results in the absence of Pd were registered in the sample Zn_{50}230/72. It was also shown that specific surface area and total pore volume had the most significant influence on photocatalytic activity, while the influence of Pd co-catalyst is not so important.

Acknowledgement: Grateful acknowledgements to IOSUD-UPT (Politehnica University Timisoara) for support and to Dr. Ing. Viorel Sasca (Institute of Chemistry Timisoara of Romanian Academy) for the assistance and offered possibility to conceive GC measurements and adapt the whole system to the desired requirements.

References

1. J. Wang, B. Li, J. Chen, N. Li, J. Zheng, J. Zhao, Z. Zhu, "Enhanced photocatalytic H2-production activity of $Cd_xZn_{1-x}S$ nanocrystals by surface loading MS (M = Ni, Co, Cu) species", *Appl. Surf. Sci.*, **259** (2012) 118–123.
2. A. Kudo, Y. Miseki, "Heterogeneous photocatalyst materials for water splitting", *Chem. Soc. Rev.*, **38** (2009) 253–278.
3. X. Fu, Y. Zhang, P. Cao, H. Ma, P. Liu, L. He, J. Peng, J. Li, M. Zhai, "Radiation synthesis of CdS/reduced graphene oxide nanocomposites for visible-light-driven photocatalytic degradation of organic contaminant", *Radiat. Phys. Chem.*, **123** (2016) 79–86.
4. G. Chen, F. Li, Y. Fan, Y. Luo, D. Li, Q. Meng, "A novel noble metal-free ZnS–WS_2/CdS composite photocatalyst for H_2 evolution under visible light irradiation", *Catal. Commun.*, **40** (2013) 51–54.
5. E. Hong, D. Kim, J.H. Kim, "Heterostructured metal sulfide (ZnS–CuS–CdS) photocatalyst for high electron utilization in hydrogen production from solar water splitting", *J. Ind. Eng. Chem.*, **20** [5] (2014) 3869–3874.
6. C.V. Reddy, J. Shim, M. Cho, "Synthesis, structural, optical and photocatalytic properties of CdS/ZnS core/shell nanoparticles", *J. Phys. Chem. Solids*, **103** (2017) 209–217.
7. D.S. Rane, L.A. Patil, "Studies on structural and optical properties of Cu doped $Cd_xZn_{1-x}S$ thin films by spray pyrolysis", *AIP Conf. Proc.*, **1451** (2012) 295–297.
8. A.A. Ismail, D.W. Bahnemann, "Photochemical splitting of water for hydrogen production by photocatalysis: A review", *Sol. Energy Mater. Sol. Cells*, **128** (2014) 85–101.
9. V.K. Ashith, K.R. Gowrish, "Bandgap tailoring in $Cd_xZn_{1-x}S$ alloy films deposited by successive ionic layer adsorption and reaction", *Thin Solid Films*, **626** (2017) 1–8.
10. Z.Q. Qina, F.J. Zhang, "Surface decorated $Cd_xZn_{1-x}S$ cluster with CdS quantum dot as sensitizer for highly photocatalytic efficiency", *Appl. Surf. Sci.*, **285** (2013) 912–917.
11. J. Wang, B. Li, J. Chen, L. Li, J. Zhao, Z. Zhu, "Hierarchical assemblies of $Cd_xZn_{1-x}S$ complex architectures and their enhanced visible-light photocatalytic activities for H_2-production", *J. Alloys Compd.*, **578** (2013) 571–576.
12. R. Sasikala, A.P. Gaikwad, V. Sudarsan, R. Rao, Jagannath, B. Viswanadh , S.R. Bharadwaj , "The dual role of palladium in enhancing the photocatalytic activity of CdS dispersed on NaY-zeolite", *Phys. Chem. Chem. Phys.*, **17** (2015) 6896–6904.
13. H. Yao, H. Shen, X. Zhu, J. Jiao, J. Li, W. Wang, "Influence of Cd source concentration on photocurrent response property of $Cd_xZn_{1-x}S$ film prepared by chemical bath deposition", *Ceram. Int.*, **42** [2] (2016) 2466–2471.
14. J. Zhu, J. Zhang, J. Zhen, C. Chen, J. Lu, S. Chen, "Controllable synthesis of water-soluble luminescent $Cd_xZn_{1-x}S$ nanocrystals", *Physica B: Condens. Matter.*, **405** (2010) 3452–3457.
15. R. Christie, *Colour Chemistry*, The Royal Society of Chemistry, UK, 2001.
16. W. Zhang, W. Gao, X. Zhang, Z. Li, G. Lu, "Surface spintronics enhanced photo-catalytic hydrogen evolution: mechanisms, strategies, challenges and future", *Appl. Surf. Sci.*, **434** (2018) 643–668.
17. S. Sain, S. Patra, S.K. Pradhan, "Microstructure and optical band-gap of mechano-synthesized $Cd_xZn_{1-x}S$ quantum dots", *J. Phys. D: Appl. Phys.*, **44** (2011) 1–8.
18. J. Tauc, *Amorphous and Liquid Semiconductors*, Plenum, New York, 1974, p. 159.
19. A.R. Bari, L.A. Patil, I.G. Pathan, D.N. Surawanshi, D.S. Rane, "Characterizations of ultrasonically prepared nanostructured ZnO powder and NH_3 sensing performance of its thick film sensor", *Procedia Mater. Sci.*, **6** (2014) 1798–1804.
20. M. Chen, P. Wu, Y. Zhu, S. Yang, Y. Lu, Z. Lin, "Enhanced photocatalytic H_2 production activity of CdZnS with stacking faults structure assisted by ethylenediamine and NiS", *Int. J. Hydrog. Energy*, **43** (2018) 10938–10949.
21. Z. Liu, G. Liu, X. Hong, "Influence of surface defects and palladium deposition on the activity of CdS nanocrystals for photocatalytic hydrogen production", *Acta Phys. - Chim. Sin.*, **35** (2019) 215–222.